Applied Catalysis B: Environmental 199 (2016) 282–291

Contents lists available at ScienceDirect

Applied Catalysis B: Environmental

journal homepage: www.elsevier.com/locate/apcatb

# Plasmonic resonance nature of Ag-Cu/$TiO_2$ photocatalyst under solar and artificial light: Synthesis, characterization and evaluation of $H_2O$ splitting activity

M. Kotesh Kumar[b], K. Bhavani[b], G. Naresh[b], B. Srinivas[b], A. Venugopal[a,b,*]

[a] CSIR-Network Institute of Sustainable Energy (CSIR-NISE), India
[b] Catalysis Laboratory, Inorganic and Physical Chemistry Division, CSIR – Indian Institute of Chemical Technology, Hyderabad 500 007, Telangana, India

ARTICLE INFO

*Article history:*
Received 3 February 2016
Received in revised form 16 June 2016
Accepted 19 June 2016
Available online 23 June 2016

*Keywords:*
Plasmon resonance
$H_2O$ splitting
$H_2$
Ag-Cu alloy
$H_2$-TPR
Solar light

ABSTRACT

A reaction mechanism has been elucidated on Ag and/or Cu supported on mixed phase (anatase/rutile) of $TiO_2$ and the $H_2$ evolution rates are rationalized by physicochemical characteristics of the fresh and used catalysts by XRD, XPS, TEM and ESR analyses. In situ reduction of Ag-Cu/$TiO_2$ catalyst is monitored by UV-DR spectral studies under natural and artificial light during $H_2O$ splitting. The $H_2$-TPR analysis emphasized an interaction between reducible mixed oxides of Ag-Cu particles. Addition of Ag dramatically decreased the band gap of Cu/$TiO_2$ and increased the absorption in the visible light region. The synergism between Ag and Cu nanoparticles generated additional active sites for enhanced $H_2$ yields. A strong interaction between Ag and Cu leads to metal sites (Ag, Cu and/or Ag-Cu) act as electron traps and facilitated electron-hole separation consequently the Ag-Cu/$TiO_2$ sustained longer time.



## 1. Introduction

Increase in global warming due to the utilization of fossil fuels (finite and non-renewable); hydrogen has been identified as an ideal future energy source due to its high energy content and zero emission [1]. Currently the majority of hydrogen demands are sourced from steam reforming of natural gas; however, this process does not mitigate dependence on fossil fuels and generates large amount of carbon dioxide. One of the alternate methods to produce $H_2$ can be photocatalytic $H_2O$ splitting using infinite energy source (renewable) i.e. solar light [2]. Therefore, the development of semiconductor-based photocatalytic water splitting has been proposed as a future prospect. However, there are some limitations on $H_2$ yields with respect to low surface area of photocatalysts, fast recombination of electron/hole pairs and most importantly, the photocatalysts are active only under UV irradiation. Among the various oxide photocatalysts; $TiO_2$ is still remains the most promising catalyst owing to its low cost, chemical inertness, non toxicity and higher photo stability. Nevertheless, the wide spread use of $TiO_2$ is limited due to the wide band gap (3.2 eV, anatase crystalline $TiO_2$), which require ultraviolet (UV) irradiation thus limiting the photocatalytic activity under visible light irradiation.

Noble metal nanoparticles, such as gold, silver, platinum and palladium possess the ability to absorb visible light due to localized surface plasmonic resonance (LSPR) and therefore may also activate wide band gap semiconductors (e.g. $TiO_2$) towards visible light [3–5]. Park et al. have studied the decomposition of 50% aqueous methanol solution for hydrogen production over Ag/$TiO_2$ catalyst with rutile $TiO_2$ using low energy UV lamps [6,7]. The Cu/$TiO_2$ catalysts showed reasonably good photocatalytic activity using sacrificial reagents to produce $H_2$, since Cu species facilitated the charge separation and provided the reduction sites [8]. The bimetallic doped $TiO_2$ may exhibit synergetic effect on photocatalytic property which is different from mono metallic catalysts. The bimetallic component plays an important role in the photocatalytic activity e.g. (i) it would shift the optical response of the $TiO_2$-based catalyst from UV to visible region, (ii) improve the electron-hole separation and function as a co-catalyst.

The bimetallic copper and silver nano colloids explored for Escherichia coli degradation [9], for antimicrobial activity [10], antibacterial investigation of silver-copper [11] and for aerosol reactor [12]. Kobayashi et al. have synthesized Ag-Cu alloy nanoparticles by reducing with hydrazine and citric acid as stabilizer at

* Corresponding author at: Catalysis Laboratory, Inorganic and Physical Chemistry Division, CSIR – Indian Institute of Chemical Technology, Hyderabad 500 007, Telangana, India.
*E-mail address:* akula@iict.res.in (V. A.).

http://dx.doi.org/10.1016/j.apcatb.2016.06.050
0926-3373/

**Table 1**
Physicochemical characteristics of the mono (Ag and/or Cu) and bimetallic (Ag-Cu) photocatalysts.

| Photocatalyst | Metal loading (wt%) | | Calcination temperature (°C) | Band gap (eV)[a] | BET-surface area ($m^2g^{-1}$) | Phase composition[b] (%) | | Crystallite size (nm)[b] | | $N_2O$ uptake ($\mu mol/g_{cat}$) | Metal particle size (nm)[c] | $H_2$ uptake ($mmol/g_{cat}$) | |
|---|---|---|---|---|---|---|---|---|---|---|---|---|---|
| | Ag | Cu | | | | Anatase | Rutile | Anatase | Rutile | | | Fresh[d] | Photo reduced[e] |
| $TiO_2$-P25 | 0.0 | 0.0 | 450 | 3.20 | 56.0 | 80 | 20 | 21 | 15 | nf | | | |
| 0.5wt%Ag/$TiO_2$ | 0.5 | 0.0 | 450 | 2.97 | 43.2 | 78 | 22 | 14 | 22 | nf | 0.95 | 36.5 | 25.4 |
| 2wt%Cu/$TiO_2$ | 0.0 | 2.0 | 450 | 3.06 | 45.7 | 81 | 19 | 17 | 16 | 3.45 | 0.54 | 108.8 | 63.7 |
| 0.5wt%Ag-2wt%Cu/$TiO_2$ | 0.5 | 2.0 | 350 | 2.92 | 40.9 | 77 | 23 | 16 | 14 | – | | | |
| 0.5wt%Ag-2wt%Cu/$TiO_2$ | 0.5 | 2.0 | 450 | 2.91 | 35.1 | 82 | 18 | 17 | 14 | 3.15 | 0.47 | 347.0 | 272.4 |
| 0.5wt%Ag-2wt%Cu/$TiO_2$ | 0.5 | 2.0 | 550 | 2.88 | 30.4 | 84 | 16 | 18 | 16 | – | | | |
| 0.5wt%Ag-2wt%Cu/$TiO_2$ | 0.5 | 2.0 | 650 | 2.84 | 19.3 | 36 | 64 | 14 | 27 | – | | | |
| 0.5wt%Ag-2wt%Cu/$TiO_2$ | 0.5 | 2.0 | 750 | 2.82 | 11.5 | 19 | 81 | 13 | 27 | – | | | |

nf: not found.
[a] Measured from UV-DRS.
[b] Measured from XRD spectra.
[c] Measured from ESR spectra [31].
[d] Measured from $H_2$-TPR with a calibrated $Ag_2O$ TPR.
[e] $H_2$ uptake of the photo reduced (10 h) samples.

room temperature [13]. Liu et al. reported Plasmon enhanced photo-electrochemical activity of Ag-Cu nanoparticles on $TiO_2$ [14]. A lot of work has been reported on the preparation of noble metal alloys, there are very few reports on bimetallic Ag-Cu for the production of hydrogen under natural solar light. The objective of this study is to reduce the band gap of the photocatalyst for enhanced visible light absorption. All the catalysts were characterized by various spectroscopic techniques and the $H_2$ evolution rates are correlated with Cu metal surface areas obtained by $N_2O$ decomposition studies. EDAX analysis of the mono and bimetallic samples revealed that Ag and Cu compositions are in close range to the nominal loadings suggesting that there is no metal loss during the preparation and activation (Table S1).

## 2. Experimental

### 2.1. Materials and reagents

Titanium dioxide nano particles ($TiO_2$-P25) consists of 80% anatase and 20% rutile phase with surface area of 50 $m^2 g^{-1}$ and a particle size of 21 nm was procured from Degussa Corporation, Germany. Methanol, copper nitrate and silver nitrate (AR grade) were obtained from sigma Aldrich. The millipore grade water was used for all the experiments in this study.

### 2.2. Preparation of catalysts

The mono and bimetallic catalysts were prepared by wet impregnation method. In a typical method required amounts of aqueous Ag and/or Cu salt solutions were impregnated on $TiO_2$-P25 to give corresponding wt% e.g. 0.5, 1 and 2 of Ag and/or Cu. The obtained suspension was stirred for 30 min and then dried in an oven at 100 °C for about 12 h. The dried solid powder was calcined in static air at 450 °C for 3 h at a rate of 5 °C $min^{-1}$. In some case the catalysts were calcined at various temperatures ranged from 350 to 750 °C in static air for 3 h. The individual samples with a loading of Ag (0.5, 1, 2, 3 wt%) and Cu (0.5, 1, 2, 3 wt%) were prepared for the comparison under similar protocol.

### 2.3. Characterization of catalysts

The catalyst samples were characterized by powder XRD, BET-SA, TEM, XPS, FT-IR, $H_2$-TPR, UV-DRS, ESR, Cyclic Voltammetry and Raman spectroscopy. The experimental conditions adopted in this investigation using the above techniques are similar to what was reported by us recently [15].

### 2.4. Evaluation of catalysts

The photocatalytic $H_2O$ splitting experiments were carried out in an air tight quartz reactor (capacity: 150 mL) using pure water and/or in aqueous methanol solution (methanol as scavenger) at ambient temperature under the natural solar irradiation (between 7 AM to 5 PM Sunny days, Hyderabad, India) and also using artificial solar irradiation (Solar Simulator, artificial Sun A.M1.5 Make: Sciencetech, Ontario, Canada). Solar light intensity was measured using the digital lux meter and the average light intensity was approximately *ca.*1,30,000 lx. In a typical experiment, required amount of catalyst was suspended in a 50 mL of pure water and/or the 10 vol.% aqueous methanol sealed with an air tight rubber septum (Aldrich) and the solution was magnetically stirred for at least 30 min to ensure the uniformity of the system. Then the reactor was purged with high purity nitrogen gas to remove the dissolved gases in the solution and the purging continued to ensure an inert atmosphere in the reactor. Prior to the photoreaction, the suspension was magnetically stirred in the dark for 30 min to establish

an adsorption/desorption equilibrium. Subsequently the aqueous suspension contained water and/or aqueous methanol was then irradiated by artificial light and/or natural solar light under constant stirring. At regular time intervals the hydrogen produced was analyzed by a gas chromatograph (GC) with thermal conductivity detector (TCD) using molecular sieve 5A packed column and $N_2$ as a carrier gas.

The recycle studies were carried out in order to evaluate the stability of the photocatalyst for 5 cycles. The 1st cycle of experiment was carried out for ~10 h under light irradiation, and the reactor was kept in the dark over night with air tight at room temperature. Prior to 2nd cycle, the gaseous products in the reactor was evacuated and then purged with nitrogen gas to ensure the absence of $H_2$ and $O_2$ by GC analysis and the experiment was performed for 10 h. The same procedure was repeated for all the subsequent recycle experiments.

## 3. Results

### 3.1. BET – surface area and XRD analysis

The XRD patterns of the calcined monometallic (0.5wt%Ag/$TiO_2$, 2wt%Cu/$TiO_2$) and bimetallic (0.5wt%Ag-2wt%Cu/$TiO_2$) catalysts (Fig. S1A) showed diffraction lines due to anatase $TiO_2$ at 25° (major), 37°, 48°, 55°, 56°, 62°, 71° and 75° and the rutile $TiO_2$ phase at 28° (major), 36°, 42° and 57°. Absence of diffraction peaks corresponding to Ag and Cu phases may probably due to low concentration of these metals or their crystalline size may be below the X-ray detection limit [16]. The XRD results of 0.5wt%Ag-2wt%Cu/$TiO_2$ catalyst calcined at different temperatures (Fig. S1B) is reported in Table 1. Calcination temperature has strong influence on crystallite size and phase composition of both rutile and anatase $TiO_2$. With increase in calcination temperature from 350 to 550 °C, the diffraction peaks became sharp indicating the increased crystallite size of both anatase and rutile. Further increase from 550 to 750 °C, resulted in strong and intense crystal of rutile phase at the cost of anatase. The calcination temperature at and above 650 °C leads to phase transformation of anatase to rutile $TiO_2$ occurred. The BET-surface area of mono and bimetallic (Ag-Cu) catalysts are lower than the bare $TiO_2$; which is possibly due to pore blockage of $TiO_2$ with Ag, Cu and/or Ag-Cu species. Diffraction lines attributed to Ag-Cu alloy is found in the used catalysts emphasizing the photo reduction of the catalyst during the course of reaction (Fig. S2). It was also well recognized that CuO and $Ag_2O$ alloy possesses easily phase separation, due to the radius inequality between Cu and Ag within the alloy-nanoparticles [17]. The diffraction peak appeared around 41°, (Fig. S2) is an indication of formation of alloy [18].

### 3.2. UV–vis DRS analysis

The optical response of 2wt%Cu/$TiO_2$, 0.5wt%Ag/$TiO_2$ and 0.5wt%Ag-2wt%Cu/$TiO_2$ nanoparticles are represented in Fig. S3. The absorption maxima for mono and bimetallic (silver and copper impregnated $TiO_2$-P25) nanoparticles are red shifted. A significant increase in the absorption region at wave lengths shorter than bare $TiO_2$-P25 is attributed to the intrinsic absorption of $TiO_2$ with band gap of 3.2 eV. Upon doping of silver and/or copper the band edge of $TiO_2$ is slightly expanded into the visible region, which is explained by the additional energy levels created by Ag and/or Cu ions in the $TiO_2$ crystal.

The Ag and/or Cu samples showed a long tail extending up to 430, 450 and 500 nm for 2wt%Cu/$TiO_2$, 0.5wt%Ag/$TiO_2$ and 0.5wt%Ag-2wt%Cu/$TiO_2$ respectively. The Ag loaded $TiO_2$ exhibited an absorption band in the visible region ~380 nm. Expansion of $TiO_2$ band edge into visible region by doping of Ag may be due to the increased number of electronic states in the surface lattice by the interaction of Ag particles with $TiO_2$ [19]. The 2wt%Cu/$TiO_2$ catalyst showed an absorption band at ~630 nm which is in good agreement with the intrinsic absorption of CuO species [20]. The shift in absorption maxima is strong on 0.5wt%Ag-2wt%Cu/$TiO_2$ compared to 2wt%Cu/$TiO_2$ and 0.5wt%Ag/$TiO_2$ samples [Table 1].

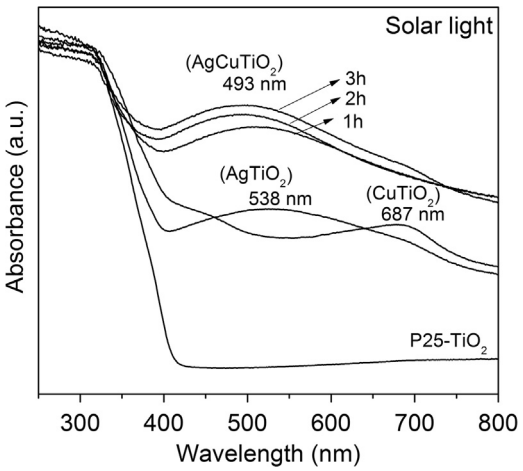


**Fig. 1.** Surface plasmonic resonance of mono (Ag and/or Cu) and bimetallic (Ag-Cu) supported on $TiO_2$ samples recovered after solar light exposure.

The 0.5 wt%Ag-2wt%Cu/$TiO_2$ demonstrated absorption band at 493 nm which is quite different from mono metallic (Ag and/or Cu/$TiO_2$) samples and is blue shifted [21]. Nature of bimetallic nanoparticles depends critically on their size, shape, composition and structure, either as alloy or core-shell. The 0.5wt%Ag/$TiO_2$ and 2wt%Cu/$TiO_2$ samples exhibited surface plasmonic resonance (SPR) bands approximately at 538 and 687 nm, respectively (Fig. 1). It is noticed that the intensity of SPR of 0.5wt%Ag-2wt%Cu/$TiO_2$ photocatalyst is changed with irradiation time. The absorption signal at 493 nm is an indication of Ag-Cu alloy [22,23]. The intensity of SPR of the samples is changed with irradiation time due to the reduction of metal oxide to metal over a period of illumination. The $Ag_2O$ and CuO species undergo reduction as the irradiation time progress, as a result the absorption bands emerged at high energy region (blue shift). With the irradiation time progress, the rate of reduction of metal oxide to metal seems to increase consequently enhanced SPR peak is observed (Fig. 1). The UV-DRS analysis of the fresh (as synthesized samples) did not show any signals in the 400–800 nm region which indicates that the metal oxides does not exhibit SPR (Fig. S3A).

The intensity increases within the range with time (0–10 h) on irradiation. The increase in surface plasmon resonance peaks for each nano alloy as observed by Abdul Salam et al. by varying the molar concentration of $Ag^+$ and $Cu^{2+}$ ions [22]. It was observed that the position of the SPR peak is shifted toward the blue region when the concentration of the silver ion in the electrolyte is increased. The molar concentration of copper ion is increased the peak position is shifted toward the red region in the UV–vis spectrum [22]. The 0.5wt%Ag-2wt%Cu/$TiO_2$ catalyst has undergone photo reduction during the course of reaction as a result the band gap is decreased both in solar and artificial light irradiation (Fig. 2). The XRD results further confirmed the formation of Ag-Cu alloy species under light irradiation over Ag-Cu/$TiO_2$ (Fig. S2).

### 3.3. $H_2$-temperature programmed reduction (TPR)

Fig. 3 shows the TPR profiles of 0.5wt%Ag/$TiO_2$, 2wt%Cu/$TiO_2$ and 0.5wt%Ag-2wt%Cu/$TiO_2$ samples. The TPR pattern of 0.5wt%Ag/$TiO_2$ (Fig. 3a) showed a peak at $T_{max}$ ~120 °C, due

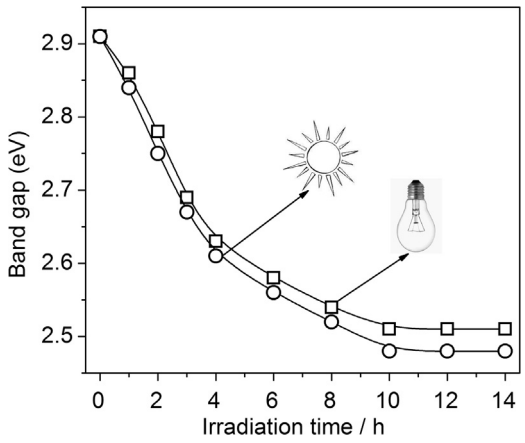


**Fig. 2.** In-situ reduction of 0.5wt%Ag-2wt%Cu/$TiO_2$ (with time) during photocatalytic $H_2O$ splitting.

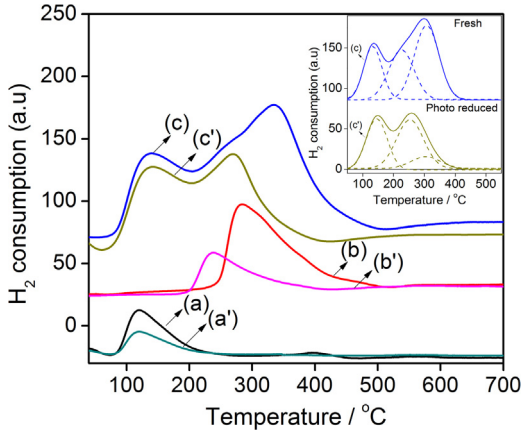


**Fig. 3.** $H_2$-TPR patterns of (a) 0.5wt%Ag/$TiO_2$ (b) 2wt%Cu/$TiO_2$ and (c) 0.5wt%Ag-2wt%Cu/$TiO_2$ fresh and photo reduced (a′) 0.5wt%Ag/$TiO_2$ (b′) 2wt%Cu/$TiO_2$ and (c′) 0.5wt%Ag-2wt%Cu/$TiO_2$ samples.

to the reduction of $Ag_2O$ to Ag [24]. The low temperature reduction signal is attributed to finely dispersed silver particles. A small hump around 390 °C is assigned to large clusters of Ag particles. The 2wt%Cu/$TiO_2$ indicated a strong peak at $T_{max}$ ~284 °C due to $Cu^{2+}$ to $Cu^0$ with a shoulder around 450 °C (Fig. 3b) [25]. The 0.5wt%Ag-2wt%Cu/$TiO_2$ (Fig. 3c) clearly showed an interaction between Ag and Cu particles as the $T_{max}$ of $Ag_2O$ drifted towards higher and the $Cu^{2+}$ reduction peak shifted to lower temperatures. Therefore, the high temperature reduction peak is attributed to Cu-Ag alloy particles having strong interaction with support. A shoulder from the low temperature region (Fig. 3c) around 250 °C are easily reducible $Cu^{2+}$ and the high temperature peak can be assigned to segregated large sized CuO particles, or possibly due to Cu catalyzed reduction of $TiO_2$ to $Ti^{3+}$ ions [26]. Hence the enhanced $H_2$ uptake on Ag-Cu/$TiO_2$ not only due to combined $Ag_2O$ reduction but also contributed from the reduction of $TiO_2$ to $Ti^{3+}$ species. Apparently shift in $T_{max}$ of silver oxide (to high temperature) and ionic Cu to lower temperatures confirming the interaction between Ag-Cu and also with the $TiO_2$. These results thus emphasized the presence of Ag-Cu reducible species along with segregated $Ag_2O$ and CuO particles. Hence the reduction peak around 280–330 °C can be Ag-Cu mixed oxide particles. The standard reduction potential of $Cu^{2+}/Cu^0$ (+0.34 V) is relatively low compared to $Ag^+/Ag^0$ (+0.78 V) as a result $Ag_2O$ particles were reduced rapidly than the CuO particles. The reduction profiles (Fig. 3) clearly distinguish the reduction peaks for $Ag_2O$ and CuO

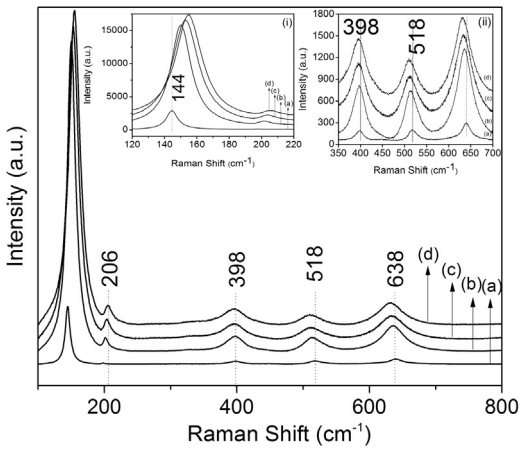


**Fig. 4.** Raman spectra of (a) P25-$TiO_2$, (b) 0.5wt%Ag/$TiO_2$, (c) 2wt%Cu/$TiO_2$, (d) 0.5wt%Ag-2wt%Cu/$TiO_2$ photocatalysts.

in 0.5wt%Ag-2wt%Cu doped $TiO_2$ sample and confirming that a bimetallic alloy has been formed [27].

### 3.4. XPS analysis

The X-ray photoelectron spectra of fresh 0.5wt%Ag-2wt%Cu/$TiO_2$ catalyst (Fig. S4) shows signals at a binding energy (BE) of (530.6 eV, 531.7 eV); (458.8 eV, 465.2 eV); (934.1 eV, 954.6 eV) and (368.1 eV, 373.8 eV) are corresponding to O 1s, Ti 2p, Cu 2p and Ag 3d respectively. The BE values of these species are in agreement with the reported literature [28]. The O 1 s spectra (Fig. S4a) showed two signals contributed from Ti-O-Ti (lattice oxygen) and −OH (hydroxyl oxygen) respectively [29]. Two well-resolved peaks at 465.2 and 458.8 eV (Fig. S4b), assigned to Ti $2p_{1/2}$ and Ti $2p_{3/2}$ spin-orbital components in $TiO_2$, corresponding to $Ti^{4+}$ in a tetragonal structure. Fig. S4c shows the characteristic Cu 3d peaks attributed to surface ($Cu^{2+}$) species. The position of Ti 2p peaks shifted to slightly lower BE in the presence of CuO in consistent with literature result [30]. The binding energy of Ag $3d_{5/2}$ and $3d_{3/2}$ are the characteristic signals of interacted $Ag^+$ ions (Fig. S4d) with the surface hydroxyl groups of $TiO_2$ [31,32].

### 3.5. Raman spectroscopic analysis

The Raman spectra of 0.5wt%Ag/$TiO_2$, 2wt%Cu/$TiO_2$ and 0.5wt%Ag-2wt%Cu/$TiO_2$ catalysts (Fig. 4) revealed strong vibrational bands at 401 ($B_{1g}$), 515 ($B_{1g}$) and 638 $cm^{-1}$ ($E_g$) assigned to $TiO_2$ [33]. The Ti-O-Ti network bands in the region 400–700 $cm^{-1}$ are characteristic of anatase and rutile structure. Typically, three Raman active fundamental modes for anatase phase are appeared at 397 $cm^{-1}$ ($B_{1g}$), 518 $cm^{-1}$ ($A_{1g} + B_{1g}$) and 640 $cm^{-1}$ ($E_g$) and rutile $TiO_2$ at 613 $cm^{-1}$ ($A_{1g}$) [34]. Furthermore, the band at 144 $cm^{-1}$ shifted towards higher wave number (inset Fig. 4(i)), while the 640 $cm^{-1}$ peak drifted downwards to lower wave number (inset Fig. 4(ii)) is presumably due to the interaction of mono and/or bi metallic species with $TiO_2$ [35].

### 3.6. Electron spin resonance (ESR) analysis

The ESR spectra of 0.5wt%Ag/$TiO_2$, 2wt%Cu/$TiO_2$ and 0.5wt%Ag-2wt%Cu/$TiO_2$ (fresh) samples are reported in Fig. 5. A weak ESR signal appeared in 0.5wt%Ag/$TiO_2$ may be explained by $Ti^{3+}$ species in the sample (Fig. 5a). A strong axially symmetric signal is attributed to highly dispersed $Cu^{2+}$ ions on the $TiO_2$ (Fig. 5b and c). Long-range dipolar coupling (dipole–dipole interactions) between $Cu^{2+}$ ions in large grain CuO particles causes broadening of ESR

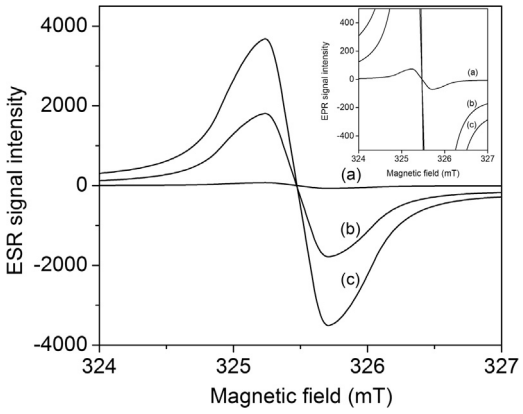


**Fig. 5.** ESR spectra of (a) 0.5wt%Ag/$TiO_2$, (b) 2wt%Cu/$TiO_2$ and (c) 0.5wt%Ag-2wt%Cu/$TiO_2$ photocatalysts.

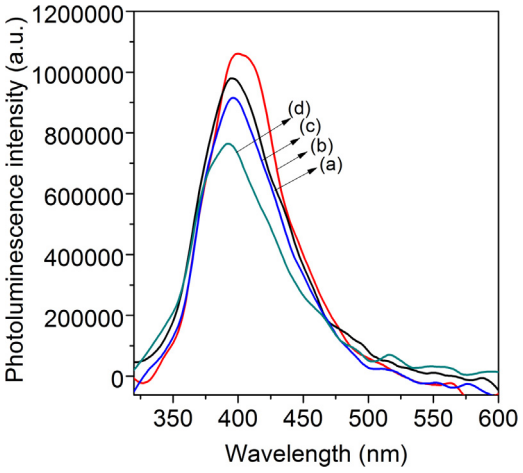


**Fig. 6.** Photoluminescence spectra of (a) 0.5wt%Ag/$TiO_2$, (b) 2wt%Cu/$TiO_2$, (c) 0.5wt%Ag-2wt%Cu/$TiO_2$ fresh and (d) 0.5wt%Ag-2wt%Cu/$TiO_2$ (recovered after reaction) samples.

spectral lines. According to Kawabata hypothesis, the broadening of ESR signal of nano metal particles is affected by the quantum size effect and can be correlated to the size of the nano metal particle [36]. Accordingly, direct relationship between the line width $\Delta H_{pp}$ ($\Delta H_{pp}$ = peak-to-peak width) of the signal of nano particle in ESR spectra and its particle size is given in the following relation

$$d = a(\Delta H_{pp})^{0.5}$$

where d is the particle size in nm, $\Delta H_{pp}$ is the line width of ESR signal in mT, and "a" is the proportionality constant. The proportionality constant "a" was previously determined as 1.4 and 0.8 for Ag and Cu respectively [37]. The normalized ESR spectra indicated a similar ΔHpp ~0.46 mT over all the samples and the particle size measured using the above formula resulted to 0.95, 0.54 and 0.47 nm for Ag, Cu and $(Ag\text{-}Cu)_{alloy}$ respectively.

### 3.7. Photoluminescence spectroscopic analysis

The photoluminescence (PL) emission spectra can be used to investigate the efficiency of charge carrier trapping, immigration, transfer and to understand the fate of electron-hole pairs in semiconductors, since PL emission results from the recombination of free carriers either directly (band-band) or indirectly via a band gap state. The PL emission peaks were obtained within the visible range with peak positions at 350–550 nm [38].

The photoluminescence (PL) spectra of fresh 0.5wt%Ag/$TiO_2$, 2wt%Cu/$TiO_2$, 0.5wt%Ag-2wt%Cu/$TiO_2$ and used 0.5wt%Ag-2wt%Cu/$TiO_2$ (recovered after reaction) photocatalysts are reported in Fig. 6. It shows two common signals cantered around 390 and 420 nm are assigned to emission of band gap transitions of anatase and rutile phases of $TiO_2$ respectively. The small intense peaks in the low energy region are ascribed to excitonic signals originating from oxygen vacancies and defects on the catalyst surface [39]. The 2wt%Cu/$TiO_2$ sample showed slightly higher PL intensity than the 0.5wt%Ag/$TiO_2$. In contrast the fresh 0.5wt%Ag-2wt%Cu/$TiO_2$ exhibited higher PL intensity than the used catalyst. The decrease in PL intensity is probably due to electron capture by the metals (Ag and/or Cu) from the $TiO_2$ conduction band. These observations are in good agreement with the results reported by Kim and Kang in the photoluminescence spectra of Cu-Ag-$TiO_2$ catalysts [40]. The TPR analysis (Fig. 3) of the photo reduced samples indicated a decrease in $H_2$ uptake, which is due to the partially reduced Ag and/or Cu or the mixed oxides of $Ag_2O$-CuO during the irradiation. These results further supplement the lower PL signal intensity of 0.5wt%Ag-2wt%Cu/$TiO_2$ used catalyst due to a higher number of oxygen vacancies and defects formed during the photo reduction of the catalyst [41].

## 4. Discussion

### 4.1. Mechanism of $H_2O$ splitting

During illumination the $TiO_2$ composed of both anatase and rutile phases simultaneously activated to generate holes ($h^+$) in valance band and electrons ($e^-$) in the conduction band. The holes are consumed by either water/methanol at valance band of rutile $TiO_2$ leading to generation $H^+$ ions. Under the illumination the electrons ($e^-$) are populated more in the conduction band of anatase $TiO_2$ as the conduction potential of rutile $TiO_2$ is 0.2 V higher than anatase $TiO_2$. Thus generated electrons in rutile phase are transferred to conduction band of anatase $TiO_2$, and these electrons reduce the $H^+$ ions leading to molecular hydrogen [42]. Meanwhile the hole present at valance band of anatase $TiO_2$ is transferred to valance band of rutile $TiO_2$ as shown in Scheme 1.

The $TiO_2$ (P-25 Degussa) is a standard photocatalyst owing to its wide band gap energy of ~3.2 eV and will be activated in the ultraviolet region. Under natural solar light (~only 5% UV radiation available), the $TiO_2$ (P-25) demonstrated very low *ca.* 271 μmol $g^{-1}$ of $H_2$. Using a Solar Simulator (artificial solar lamp, the instrument is equipped with UV light filtration) a further decrease in $H_2$ yield ca. 102 μmol $g^{-1}$ is observed. The two major crystalline phases of $TiO_2$ investigated as photocatalysts in this study are anatase and rutile, with a band gap of ca. 3.2 and 3.0 eV, respectively [43,44]. The rutile phase is the most chemically stable phase of $TiO_2$ and the anatase is generally regarded as the more active phase than rutile [45]. The mixed-phase of $TiO_2$ i.e. commercial Degussa P25 was found to exhibit enhanced photocatalytic properties in contrast to either anatase or rutile $TiO_2$. Li and co-workers proposed the formation of a surface junction between anatase and rutile that is responsible for the enhanced photocatalytic activity of mixed phase of $TiO_2$ [46]. The rate of hydrogen production using pure water is very low (20 μmol $g^{-1}$) which is due to the fast recombination of charge carriers ($e^-$, $h^+$). We have observed that the life time of charge carriers improved upon using the biphasic (anatase/rutile) junction in presence of scavenger/sacrificial reagent i.e. methanol. It is clearly evident that the rate of $H_2$ is less in pure water than in presence of sacrificial reagent. It has been reported that both water and methanol undergo oxidation at the holes since the oxidation potential of $TiO_2$ is much higher than the oxidation potential of water as well as methanol i.e. 1.23 and 0.55 eV respectively [47,48].

Charge separation could be achieved in the anatase/rutile phase junction as a result prolonged lifetime of charge carriers would

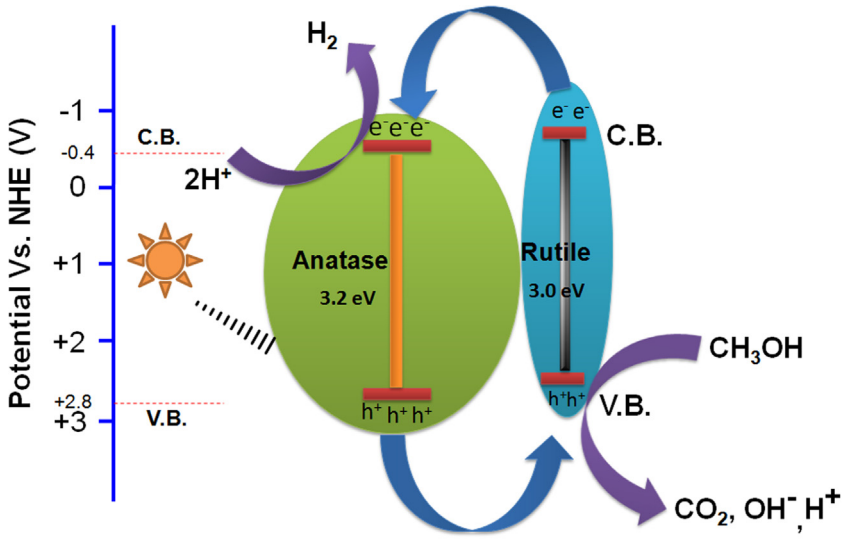


**Scheme 1.** Hydrogen production and electron transfer in mixed phase (anatase/rutile) of $TiO_2$.

assist an improved photocatalytic activity. Hence determination of the charge transfer process at the anatase/rutile phase junction is of great significance to reveal the role of each phase in the junction to achieve higher $H_2$ yields. Therefore, the Ag and/or Cu doped $TiO_2$ catalysts were examined under natural solar light irradiation using methanol as a hole scavenger.

### 4.2. Activity studies on $Ag/TiO_2$ catalysts

Fig. S6 represents the effect of Ag loadings on $TiO_2$ in the photocatalytic hydrogen production using methanol and water mixture. The $TiO_2$ displayed lower $H_2$ production than the $Ag/TiO_2$ catalyst. Doping of Ag on $TiO_2$ resulted in a substantial improvement in the $H_2$ evolution. When the Ag loading increased above 0.5 wt%, the photocatalytic activity is decreased gradually. At higher Ag loadings more $TiO_2$ surface is covered that would hinder the contact between $TiO_2$ and scavenger, as a result an increase in diffuse distance there by rate of hydrogen would be decreased (Fig. S6) [49]. Vamathevan et al. found that nano sized silver particles on $TiO_2$ could enhance the photocatalytic activity by a factor of 4.0 in the mineralization of sucrose [50]. In contrast, Herrmann observed that silver on $TiO_2$ did not show an increase in photocatalytic activity using single phase $TiO_2$ [51]. The bulk $Ag_2O$ has a band gap of 1.2 eV cannot produce hydrogen from pure water as it requires a minimum of 1.23 eV. Using methanol and water mixture it can produce some amount of hydrogen; however the oxide undergoes spontaneous photo corrosion. Therefore $Ag/TiO_2$ showed spectral line in the visible region that is evidenced by UV–vis DRS wherein a reduction in band gap is observed (Fig. S3). The 0.5wt%$Ag/TiO_2$ demonstrated *ca.* 5500 $\mu mol\, g^{-1}$ $H_2$ is obtained under natural solar irradiation over catalyst (Scheme 2).

### 4.3. Activity studies on $Cu/TiO_2$ catalysts

CuO has been proved to be good promoter to hybridise with $TiO_2$ with a narrow band gap of 2.0 eV that could extend the absorption to visible light range up to 620 nm. Both the conduction and valance bands of CuO lie higher than those of $TiO_2$, which is favourable for the efficient transfer of excited electrons and holes between each other (Scheme 3). Fig. S7 shows that the $H_2$ evolution rate increased with increase in Cu loading up to 2 wt% and beyond this the activity is decreased.

The TPR analysis of the photo reduced samples exhibited the reduction signals attributed to their corresponding (Ag and/or Cu) oxide species (Fig. 3). These results clearly showed a decrease in $H_2$ uptake over the photo reduced samples compared to the fresh as synthesized catalysts (Table 1). Thus confirming the presence of metallic species in the photo reduced samples. Hence a combination of both ionic and metallic particles is shown in Schemes 2 and 3. The extent of photo reduction of the oxidic (Ag and/or Cu) and Ag-Cu bimetallic catalysts are estimated from the $H_2$ uptakes of the fresh (as synthesized) and the photo reduced samples and $H_2$ uptakes are reported in Table 1. It has been observed that about 30% of metallic Ag, 41.4% of metallic Cu and 21.5% of Ag-Cu (alloy) species are present in the photo reduced samples.

### 4.4. Activity studies on $Ag\text{-}Cu/TiO_2$ catalyst

Based on the activity data on $Ag/TiO_2$ and $Cu/TiO_2$ photocatalysts which showed the ability to absorb visible light due to localized surface plasmonic resonance [52–54]; the 0.5wt%Ag-2wt%$Cu/TiO_2$ sample was evaluated under similar experimental conditions. The 0.5wt%Ag-2wt%$Cu/TiO_2$ sample calcined at 450 °C is analyzed by HRTEM and the images are reported in (Fig. 7). It shows that the lattice fringe of 0.35 nm is consistent with (101) plane of anatase $TiO_2$, while the lattice fringe of 0.23 nm is assigned to the (111) plane of $Ag_2O$ and the lattice fringe of 0.21 nm belong to the (200) plane of CuO. These results indicate the co-existence of Ag and Cu particles on the $TiO_2$ surface. It shows that the particles are with irregular morphology. The particle size is in the range of 17–21 nm.

The 2wt%$Cu/TiO_2$ demonstrated 3 times higher $H_2$ production rate compared to 0.5wt%$Ag/TiO_2$ catalyst, using methanol and $H_2O$ mixture under visible light irradiation. In the comparative analysis, 0.5wt%Ag-2wt%$Cu/TiO_2$ exhibited better $H_2$ yield than the other bimetallic compositions (Fig. 8). The higher photocatalytic activity of 0.5wt%Ag-2wt%$Cu/TiO_2$ nanoparticles may be explained by lowering of band gap. The $N_2O$ titration studies revealed a decrease in $N_2O$ uptake further emphasizing the formation of Ag-Cu alloy on the catalysts surface as the surface Ag alone did not decompose the $N_2O$ (Table 1).

Optimization of catalyst amount is essential in order to avoid excess use of catalyst and ensure total absorption of efficient photons. The effect of catalyst loading on the water splitting activity (0.5wt%Ag-2wt%$Cu/TiO_2$) is measured and the data is reported in

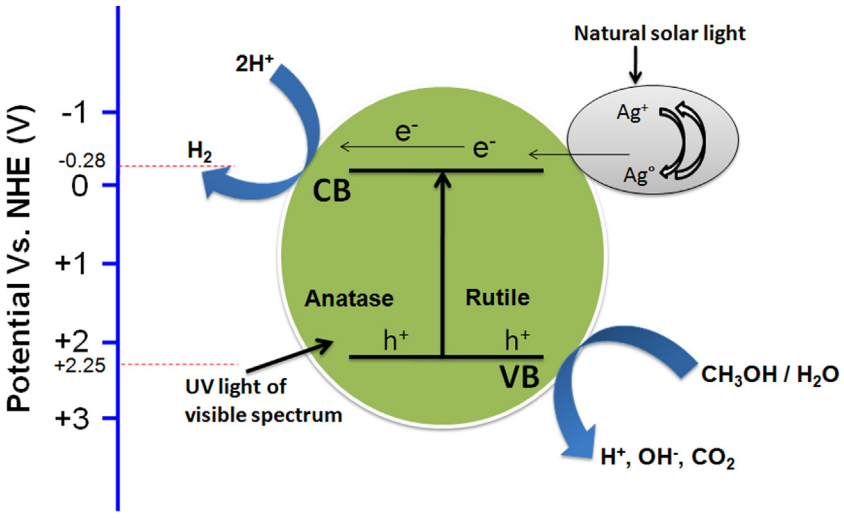


**Scheme 2.** Surface Plasmon mediated $Ag/TiO_2$ for hydrogen production under solar light irradiation.

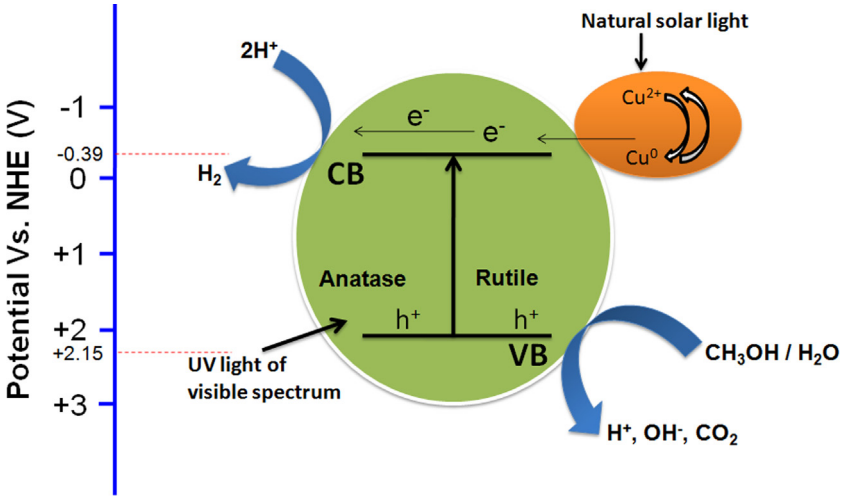


**Scheme 3.** Surface Plasmon mediated $Cu/TiO_2$ for hydrogen production under solar light irradiation.

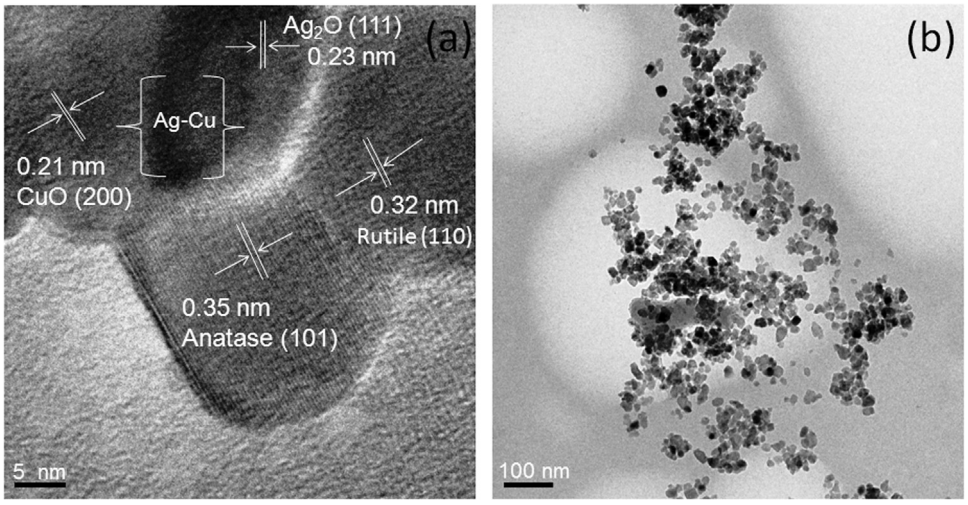


**Fig. 7.** (a) HRTEM and (b) TEM image of 0.5wt%Ag-2wt%$Cu/TiO_2$ photocatalyst.

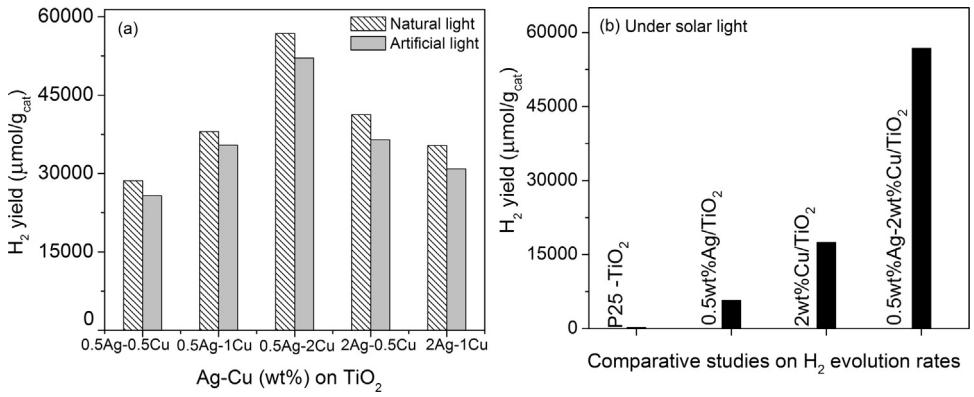


**Fig. 8.** Influence of (a) different wt% of Ag and Cu supported $TiO_2$ for $H_2O$ splitting activity under natural and artificial light irradiation (b) comparative studies on P-25 $TiO_2$, 0.5wt%Ag/$TiO_2$, 2wt%Cu/$TiO_2$ and 0.5wt%Ag-2wt%Cu/$TiO_2$ photocatalysts. Reaction conditions: ambient temperature, Time = 10 h, sacrificial reagent = 10 vol% aqueous methanol, catalyst amount ~10 mg.

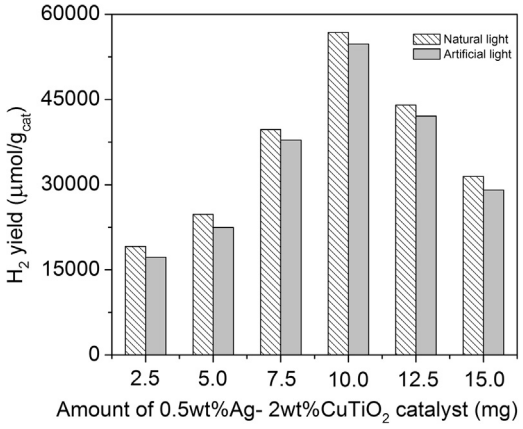


**Fig. 9.** Effect of catalyst amount on the $H_2$ evolution rates over 0.5wt%Ag-2wt%Cu/$TiO_2$. Reaction conditions: ambient temperature, Time = 10 h, sacrificial reagent = 10 vol% aqueous methanol.

Fig. 9. The initial $H_2$ rates are found to be proportional to the mass of catalyst. However, above certain loading the $H_2$ rate becomes independent of the catalyst mass. This limit corresponds to the optimum amount of Ag-Cu/$TiO_2$ at which all the catalyst particles are totally illuminated. About 10 mg of 0.5wt%Ag-2wt%Cu/$TiO_2$ catalyst has demonstrated better $H_2$ rate ~5683 μmol $g^{-1}$ $h^{-1}$ under natural solar light. The initial rates of reaction are found to be proportional to the mass of catalyst. However, above a certain amount, the reaction rate becomes independent of the mass of catalyst. This limit corresponds to the maximum amount of photo catalyst at which all particles are totally illuminated. Generally, the optimum catalyst loading must be determined in order to avoid excess use of catalyst and also to ensure total absorption of efficient photons.

Therefore, the efficiency could be enhanced with increase in Ag-Cu/$TiO_2$ load amount, since the total surface area available for methanol adsorption would increase. Further increase in the catalyst load beyond 10 mg might cause light scattering and screening effects. The excessive Ag-Cu/$TiO_2$ photocatalyst amount leads to opacity of the suspension, which prevents the catalyst in solution from being illuminated. The scattering and screening effects reduce the specific activity of the catalyst. Thus, the production of hydrogen decreases with increasing amount of the catalyst. In the present investigation, the optimum amount of catalyst was found to be 10 mg for the production of hydrogen under solar light in aqueous medium compared to artificial light irradiation.

The 0.5wt%Ag-2wt%Cu/$TiO_2$ sample demonstrated higher $H_2$ rates compared to their individual 0.5wt%Ag/$TiO_2$ and 2wt%Cu/$TiO_2$ catalysts. The high $H_2$ rate on Ag-Cu/$TiO_2$ may probably due to the formation of Schottky barriers at the interface which seem to promote the charge transfer and there by inhibiting the recombination of electron-hole pair. The dopant particles (Cu and/or Ag) seem to act as electron sink (to decrease electron-hole recombination) which would reduce the $H^+$ ions to produce $H_2$. As the loadings of Ag, Cu increased, the crystallites become large and which tend to show the bulk characteristics such as absorption of shorter wavelengths and the fast electron – hole recombination resulting in the lower rate of hydrogen production.

The photocatalytic activity of Ag-Cu alloy is dependent upon the Ag-Cu particle size (nm). However single element has not been found to meet practical applications and therefore aimed co-doping/bimetal with different metals may lead to higher activity. The promoting effect of bimetal is attributed to either the improved spatial charge separation in $TiO_2$. It is well known that the work function of metal decreases by alloying of other metal components with a lower work function. Bimetallic alloys structures deposited on $TiO_2$ possess the ability to absorb visible light, in a wide wavelength range (broad LSPR peak), and therefore reveal the highest level of activity as a result of utilization of a large amount to incident photons. On the other hand they can enhance the rate of trapping photo excited electrons form anatase/rutile $TiO_2$ particles. Bimetallic NPs depositedon$TiO_2$ are expected to display not only the combination of the properties associated with two distinct metals, but also the new properties due to synergy between two metals inhibit the recombination process due to the capability of the storage of photo excited electrons.

The higher $H_2$ rate on bimetallic catalyst can be associated with plasmonic activation of Ag-Cu particles under visible light. The $TiO_2$ absorb UV light, while the Ag-Cu particles absorb visible light component under the solar light irradiation. The $TiO_2$ particles efficiently transfer the valance band (VB) electrons to conduction band (CB) of $TiO_2$ (anatase and/or rutile) using the UV component. Thus generated electrons in the conduction band of $TiO_2$ are transferred to Ag-Cu nano particles when in close contact with $TiO_2$. When the Ag-Cu bimetal interacts with $TiO_2$, create new energy levels at the interface to generate additional active sites for water splitting (Fig. S12) [55,56]. The improved photo catalytic performance of Ag-Cu/$TiO_2$ is explained due to their different structure and energy levels (Fig. 2). The enhanced $H_2$ yields on the bimetallic 0.5wt%Ag-2wt%Cu/$TiO_2$ catalyst is explained based on their physicochemical properties obtained from UV-DRS of photo reduced (Fig. 1), TPR (Fig. 3) and $N_2O$ decomposition studies (Table 1). We believe that the Ag-Cu particles located at the $TiO_2$ interface are highly active for $H_2O$ splitting under the visible light irradiation [57].

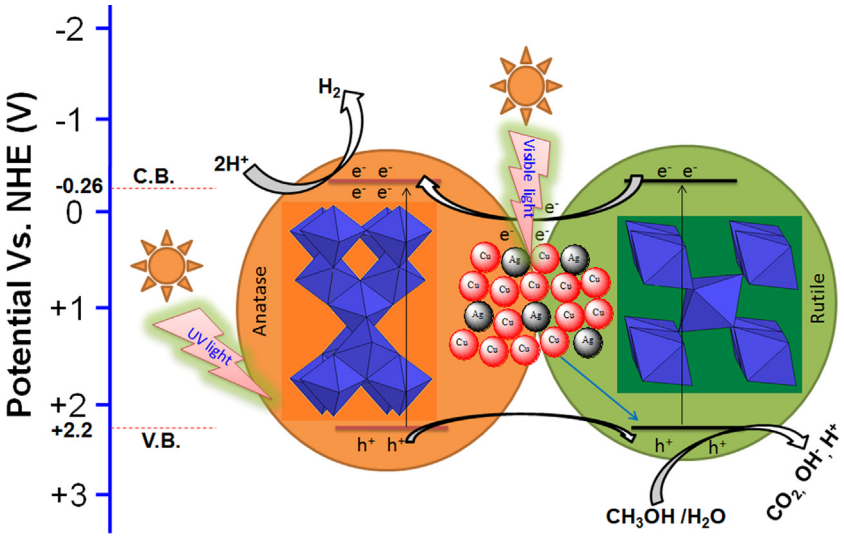


**Scheme 4.** Schematic representation of electron transfer mechanism by surface plasmonic resonance of in-situ generated Ag-Cu alloy for $H_2$ production under solar light irradiation.

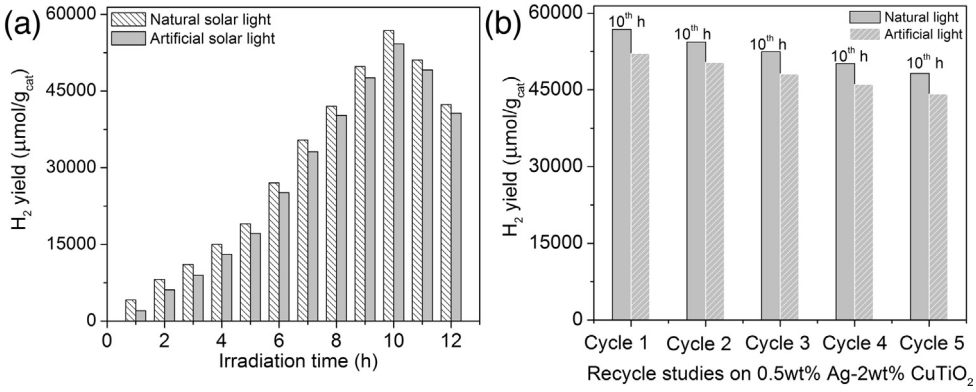


**Fig. 10.** (a) Stability studies for photocatalytic $H_2O$ splitting and (b) recycle studies over 0.5wt%Ag-2wt%Cu/$TiO_2$ photocatalysts. Reaction conditions: ambient temperature, amount of photocatalyst = 10 mg, sacrificial reagent = 10 vol% aqueous methanol.

The promotional effect of Ag-Cu particles is induced by plasmon activation under visible light followed by consecutive electron transfer from Ag-Cu to valence band of $TiO_2$ (Scheme 4). The SPR induced local electric field of activated Ag-Cu particles drive their electrons to combine with the holes on the valance band of $TiO_2$ [4]. Meanwhile, the holes created would oxidize the methanol; simultaneously reduction of $H^+$ species occurs by the conduction band electrons on the catalyst surface. Presence of Ag-Cu alloy nano particles; the bimetallic Ag-Cu/$TiO_2$ demonstrated improved photo catalytic performance under solar light which enabled efficient reduction of $H^+$ when compared to their corresponding mono metallic counterparts [58]. The bimetallic alloy particles deposited on $TiO_2$ possess the ability to absorb visible light in a wide range of wavelength due to localized surface plasmon resonance (LSPR). A strong synergism exists between the Ag and Cu seems to inhibit the recombination of holes and electrons probably due to high storage capacity of photo excited electrons by Ag-Cu alloy nano particles is a possible reason for the enhanced $H_2$ yields.

### 4.5. Effect of calcination temperature on 0.5wt%Ag-2wt%Cu/$TiO_2$ for $H_2O$ splitting

The 0.5wt%Ag-2wt%$CuTiO_2$ catalyst calcined at different temperatures examined for photocatalytic $H_2O$ splitting and the data is reported in Fig. S8. The catalyst calcined at 450 °C showed better $H_2$ yields than the other temperature. A decrease in $H_2$ yields over high temperature calcined catalysts can be explained by the agglomeration of active sites on the catalyst surface. In addition to this at higher calcination temperature transformation of anatase to rutile phase is occurred (Fig. S1B). Seery et al. have reported that thermal decomposition of $Ag_2O$ to Ag occurs on $TiO_2$ surface above 400 °C, which indicates that metallic Ag particles might have formed in all the samples calcined above 450 °C [59].

### 4.6. Effect of scavenger on 0.5wt%Ag-2wt%Cu/$TiO_2$ activity

Effect of scavenger (methanol) concentration on hydrogen evolution rate is measured over 0.5wt%Ag-2wt%Cu/$TiO_2$ catalyst under solar light irradiation (Fig. S9). Using various doses of methanol in $H_2O$; a 10 vol% $CH_3OH + H_2O$ mixture showed the maximum $H_2$ yield. Presence of excess $CH_3OH$ (15 vol%) in water exhibited drastic decrease in $H_2$ rate observed which is probably due to saturation of $CH_3OH$ on the catalyst surface [60]. It has been observed that the $H_2$ rate decreased at higher concentration of methanol. At high initial concentration of substrate, all catalytic sites are occupied and further increase in concentration does not affect the $H_2$ yield. The hydrogen production rate tends to decrease with increase in the concentration of methanol (Fig. S9).

### 4.7. Time on stream and recycle activity studies on 0.5wt%Ag-2wt%Cu/$TiO_2$

The time-on-stream analysis over 0.5wt%Ag-2wt%Cu/$TiO_2$ showed a consistent $H_2$ evolution for 10 h after which a slight decrease is found (Fig. 10a, b). This decrease may probably be due to saturation of reactor with $H_2$ that could suppress the activity. The recyclability data showed a decrease in $H_2$ yield for each subsequent cycle, which is explained by the change in pH due to oxidation of methanol to produce formaldehyde, formic acid and carbonic acid. To some extent these oxidized products affect the life time of the charge carriers ($e^-$ and $h^+$) and hence on $H_2$ yields. The comparatively decrease in photo catalytic activity may probably be due to coexistence of nano sized (anatase/rutile) in the composite material having different oxidation and reduction potentials [42]. In the presence of methanol oxidation products such as formaldehyde, formic acid and carbonic acid which may alter the pH of the solution to some extent and cause the decrease in the life time of the charge carriers ($e^-$ and $h^+$). Under optimised experimental conditions we found that there is no improvement in the $H_2$ yield while the pH is adjusted to a great extent.

## 5. Conclusions

XRD analysis of Ag-Cu/$TiO_2$ showed the conversion of anatase to rutile phase in $TiO_2$ at and above 650 °C. Reduction behaviour of the bimetallic Ag-Cu/$TiO_2$ is entirely different from its individual components due to a strong interaction between Ag and Cu particles. The UV-DRS analysis indicated a blue shift in Ag-Cu/$TiO_2$ attributed to Ag-Cu alloy species. These Ag-Cu sites are auto reduced when exposed to solar and artificial light consequently the band gap is decreased. The synergetic interaction between Ag and Cu is evident from the XRD, TPR, UV-DRS and TEM studies. The bimetallic Ag-Cu undergoes plasmonic activation in visible light, contributed to more efficient $H_2$ production in the photocatalytic $H_2O$. The Ag-Cu/$TiO_2$ demonstrated better $H_2$ yields compared to the individual Ag/$TiO_2$ and Cu/$TiO_2$ catalysts under natural and artificial light in mixture of $CH_3OH + H_2O$. The structure of Ag-Cu alloy is stable under the set of optimised experimental conditions adopted and demonstrated an amount of 5683 μmoles $g^{-1}$ $h^{-1}$ $H_2$ under natural solar light.

## Acknowledgements

The authors sincerely thank CSIR New Delhi for funding through TAPSUN program under NISE. The authors also thank Dr S Sivaram, Bhatnagar Fellow, CSIR-NCL and Prof. D. D. Sharma (IISc – Bangalore) for their constant support, encouragement and inspiration. The authors thank Dr. L. Giribabu (CSIR-IICT) for providing the photoluminescence spectra.

## Appendix A. Supplementary data

Supplementary data associated with this article can be found, in the online version, at http://dx.doi.org/10.1016/j.apcatb.2016.06.050.

## References

[1] N.Z. Muradov, T.N. Veziroglu, Int. J. Hydrog. Energy 33 (2008) 6804–6839.
[2] L. Yuan, C. Han, M.Q. Yang, Y.J. Xu, Int. Rev. Phys. Chem. 35 (2016) 1–36.
[3] X. Zhang, Y.L. Chen, R.S. Liu, D.P. Tsai, Rep. Prog. Phys. 76 (2013) 046401–046407.
[4] A. Zielinska-Jurek, J. Nanomater. 2014 (2014) 1–17.
[5] M.J. Kale, T. Avanesian, P. Christopher, ACS Catal. 4 (2014) 116–128.
[6] M.S. Park, M. Kang, Mater. Lett. 62 (2008) 183–187.
[7] J.W. Park, M. Kang, Int J. Hydrog, Energy 32 (2007) 4840–4846.
[8] J. Bandara, C.P.K. Udawatta, C.S.K. Rajapakse, Photochem. Photobiol. Sci. 4 (2005) 857–861.
[9] H.R. Ghorbani, H. Attar, S. Soltani, Indian J. Applied Pure Biol. 30 (2015) 139–142.
[10] G.M. Nazeruddin, R.N. Prasad, Y.I. Shaikh, A.A. Shaikh, Der Pharm. Lett. 6 (2014) 129–136.
[11] M. Taner, N. Sayar, I.G. Yulug, S. Suzer, J. Mater. Chem. 21 (2011) 13150–13154.
[12] M.K. Sharma, R.D. Buchner, W.J. Scharmach, V. Papavassiliou, M.T. Swihart, Aerosol Sci. Technol. 47 (2013) 858–866.
[13] R. Ferrando, J. Jelinek, R.L. Johnston, Chem. Rev. 108 (2008) 846–910.
[14] J. Liu, F. Chen, Int. J. Electrochem. Sci. 7 (2012) 9560–9572.
[15] M. Kotesh Kumar, K. Bhavani, B. Srinivas, S. Naveen Kumar, M. Sudhakar, G. Naresh, A. Venugopal, Appl. Catal. A Gen. 515 (2016) 91–100.
[16] H. Zhu, Y. Wu, X. Zhao, H. Wan, L. Yang, J. Hong, Q. Yu, L. Dong, Y. Chen, C. Jian, J. Wei, P. Xu, J. Mol. Catal. A Chem. 243 (2006) 24–30.
[17] J. Yun, K. Cho, B. Park, H.C. Kang, B.K. Ju, S. Kim, Jpn. J. Appl. Phys. 47 (2008) 5070–5075.
[18] K.R. Nemade, S.A. Waghuley, St. Petersburg Polytech. Univ. J. Phys. Math. 1 (2015) 249–255.
[19] J. Yu, J. Xiong, B. Cheng, S. Liu, Appl. Catal. B Environ. 6 (2005) 211–221.
[20] G. Colon, M. Maicu, M.C. Hidalgo, J.A. Navıo, Appl. Catal. B Environ. 67 (2006) 41–51.
[21] N.E. Motl, E. Ewusi-Annan, I.T. Sines, L. Jensen, R.E. Schaak, J. Phys. Chem. C 114 (2010) 19263–19269.
[22] A.A. Salam, R. Singaravelan, P. Vasanthi, S.B. Alwar, J. Nanostruct. Chem. 5 (2015) 383–392.
[23] M.G. Meíndez-Medrano, E. Kowalska, A. Lehoux, A. Herissan, B. Ohtani, D. Bahena, V. Briois, C. Colbeau-Justin, J.L. Rodríguez-Loípez, H. Remita, J. Phys. Chem. C 120 (2016) 5143–5154.
[24] A. Sandoval, A. Aguilar, C. Louis, A. Traverse, R. Zanella, J. Catal. 281 (2011) 40–49.
[25] N. Riaz, F.K. Chong, B.K. Dutta, Z.B. Man, M.S. Khan, E. Nurlael, Chem. Eng. J. 185–186 (2012) 108–119.
[26] P. Meriaudeau, O.H. Ellestad, M. Dufaux, C. Naccache, J. Catal. 75 (1982) 243–250.
[27] L.S. Yoong, F.K. Chong, B.K. Dutta, Energy 34 (2009) 1652–1661.
[28] L. Wu, J.C. Yu, X. Wang, L. Zhang, J. Yu, J. Solid State Chem. 178 (2005) 321–328.
[29] G. Dai, J. Yu, G. Liu, J. Phys. Chem. C 115 (2011) 7339–7346.
[30] J. Zhou, Y. Zhang, X.S. Zhao, A.K. Ray, Ind. Eng. Chem. Res. 45 (2006) 3503–3511.
[31] A. Romanyuk, P. Oelhafen, Sol. Energy Mater. Sol. Cells 91 (2007) 1051–1054.
[32] B. Ohtani, Y. Okugawa, S. Nishimoto, T. Kagiya, J. Phys. Chem. 91 (1987) 3550–3555.
[33] Z. Zhang, J.B.M. Goodall, D.J. Morgan, S. Brown, R.J.H. Clark, J.C. Knowles, N.J. Mordan, J.R.G. Evans, A.F. Carley, M. Bowker, J.A. Darr, J. Eur. Ceram. Soc. 29 (2009) 2343–2353.
[34] J. Navas, A. Sanchez-Coronilla, T. Aguilar, N.C. Hernandez, D.M.d. Santos, J. Sanchez- Marquez, D. Zorrilla, C. Fernandez-Lorenzo, R. Alcantara, J. Martin-Calleja, Phys. Chem. Chem. Phys. 16 (2014) 3835–3845.
[35] S. Sajjad, S.A.K. Leghari, F. Chen, J. Zhang, Chem. Eur. J. 16 (2010) 13795–13804.
[36] A. Kawabata, Jpn. J. Phys. Soc. 29 (1970) 902–911.
[37] M.M. Selim, H.A.E.M. Islam, Micropor. Mesopor. Mater. 85 (2005) 273–278.
[38] K. Akihiko, N. Ryo, I. Akihide, K. Hideki, Chem. Phys. 339 (2007) 104–110.
[39] J. Yu, Y. Hai, M. Jaroniec, J. Colloid Interface Sci. 357 (2011) 223–228.
[40] A.Y. Kim, M. Kang, Int. J. Photoenergy 2012 (2012) 1–9.
[41] J. Liqiang, Q. Yichun, W. Baiqi, L. Shudan, J. Baojiang, Y. Libin, F. Wei, F. Honggang, S. Jiazhong, Sol. Energy Mater. Sol. Cells 90 (2006) 1773–1787.
[42] D.O. Scanlon, C.W. Dunnill, J. Buckeridge, S.A. Shevlin, A.J. Logsdail, S.M. Woodley, C.R.A. Catlow, M.J. Powell, R.G. Palgrave, I.P. Parkin, G.W. Watson, T.W. Keal, P. Sherwood, A. Walsh, A.A. Sokol, Nat. Mater. 12 (2013) 798–801.
[43] S. Paul, A. Choudhury, Appl. Nanosci. 4 (2014) 839–847.
[44] X. Sun, W. Dai, G. Wu, L. Li, N. Guan, M. Hunger, Chem. Commun. 51 (2015) 13779–13782.
[45] U. Diebold, Surf. Sci. Rep. 48 (2003) 53–229.
[46] J. Zhang, Q. Xu, Z. Feng, M. Li, C. Li, Angew. Chem. Int. Ed. 47 (2008) 1766–1769.
[47] A. Fujishima, T.N. Rao, D.A. Tryk, J. Photochem, Photobiol. C 1 (2000) 1–21.
[48] P. Wardman, J. Phys. Chem. Ref. Data 18 (1989) 1637–1755.
[49] S.X. Liu, Z.P. Qu, X.W. Han, C.L. Sun, Catal. Today 93–95 (2004) 877–884.
[50] A. Vamathevan, R. Amal, D. Beydoun, J. Photochem, Photobiol. A 148 (2002) 233–245.
[51] J.M. Herrmann, H. Tahiri, Y. Ait-Ichou, G. Lassaletta, A.R. Gonzalez-Elipe, A. Fernandez, Appl. Catal. B Environ. 13 (1997) 219–228.
[52] C. Langhammer, Z. Yuan, I. Zoric, B. Kasemo, Nano Lett. 6 (2006) 833–838.
[53] A. Zielinska-Jurek, E. Kowalska, J.W. Sobczak, W. Lisowski, B. Ohtani, A. Zaleska, Appl. Catal. B Environ. 101 (2011) 504–514.
[54] T. Pakizeh, C. Langhammer, I. Zoric, P. Apell, M. Kall, Nano Lett. 9 (2009) 882–886.
[55] T. Arizumi, M. Hirose, N. Altaf, Jpn. J. Appl. Phys. 7 (1968) 870–874.
[56] J. Liu, F. Chen, Int. J. Electrochem. Sci. 7 (2012) 9560–9572.
[57] D. Tsukamoto, Y. Shiraishi, Y. Sugano, S. Ichikawa, S. Tanaka, T. Hirai, J. Am. Chem. Soc. 134 (2012) 6309–6315.
[58] J. Fu, S. Cao, J. Yu, J. Materiomics 1 (2015) 124–133.
[59] M.K. Seery, R. George, P. Floris, S.C. Pillai, J. Photochem. Photobiol. A Chem. 189 (2007) 258–263.
[60] N. Strataki, V. Bekiari, D.I. Kondarides, P. Lianos, Appl. Catal. B Environ. 77 (2007) 184–189.